Parameterisation of the drag effect of climbers depending on wind speed and LAD

Parameterisation of the drag effect of climbers depending on wind speed and LAD

Tess Ysebaert[a], Roeland Samson[b], Siegfried Denys[a,*]

[a] *University of Antwerp - Sustainable Energy, Air and Water Technology (DuEL), Groenenborgerlaan 171, 2020 Antwerp, Belgium*
[b] *University of Antwerp - Laboratory of Environmental and Urban Ecology, Groenenborgerlaan 171, 2020 Antwerp, Belgium*

Abstract

The implementation of green walls is increasingly seen as a strategy to tackle urban air pollution and to make cities more climate resilient. The correct description of the vegetation-wind interaction is key in describing the effect of vegetation in computational fluid dynamics (CFD) models. The accuracy of the modelled wind flow is highly linked to the uncertainty about the drag coefficient. In addition, at low wind speeds viscous drag is not negligible and it should be regarded in CFD models. This research aims to address the uncertainty related to C_d and K by including the effect of climbers on both the momentum and turbulence equations in the Wilcox revised k-ω model. The change of K with increasing Reynolds number showed an increase from $5{\cdot}10^{-8}$ m^2 up to the dynamic viscosity of air ($\approx 10^{-5}$ m^2) following a logistic function. Beyond the transition region from viscous to form drag, C_d, in the range of 0.1-1.1, declined with increasing Reynolds number following a power

*Corresponding author
URL: siegfried.denys@uantwerpen.be (Siegfried Denys)

law function. Furthermore, the plant morphological parameters determining permeability and drag coefficient were identified. This study showed that the knowledge of viscous and shape resistance is necessary to obtain accurate statistics for air flow through vegetation.
Keywords: Green walls, Computational Fluid Dynamics (CFD), Drag coefficient, Permeability, Wind tunnel validation, Leaf traits

---

Highlights

- Optimisation of vegetation effects on momentum and turbulence equations in CFD models
- Permeability of vegetation cannot be neglected at low wind speeds
- Drag coefficient declines following a power law with increasing Reynolds number
- Smaller, complex leaves and higher LAD resist air flow more at lower wind speed
- Elongated leaves and higher LAD give more resistance to air flow at higher wind speed

Abbreviations

C_d sectional drag coefficient

LAD leaf area density

Re Reynolds number

CFD computational fluid dynamics

TKE turbulent kinetic energy

SDR specific dissipation rate

RANS Reynolds-averaged Navier-Stokes

LES large eddy simulation

U_{bulk} bulk mean wind speed

LA leaf area

BA branch area

LDI leaf dissection index

FLS functional leaf size

K permeability

DE (spatial) discretisation error

GCI grid convergence index

ANOVA one-way analysis of variance

MLR multiple linear regression

1. Introduction

Vegetation is vital for the liveability in cities. The so-called urban green infrastructures, including trees, green roofs and green walls, improve air quality (Ysebaert et al., 2021), reduce the urban heat island effect (Koch et al., 2020) and noise pollution (Wong et al., 2010), and have a positive impact on biodiversity and human health (Tzoulas et al., 2007). Important in these processes is the plant's interaction with and its influence on air flow. Computational Fluid Dynamics (CFD) is increasingly being used to study these processes. Due to limitation of computing capacity and the large complexity of urban green, it has hardly been possible to resolve the flow details associated with individual plants. In large-scale atmospheric flows, the overall effect of vegetation is often included in the roughness parameters of the modified wall function. Main drawbacks are that the wind flow conditions around vegetation elements are not available and it does not include vegetation-related parameters (Belcher et al., 2003; Thom, 1969; Yang et al., 2012). Nevertheless, detailed aerodynamic information is requested to study dispersion of pollutants and thermal behaviour in urban areas. Consequently, vegetation is mostly accounted for by an explicit approach, in which vegetation is simplified as a uniform, porous medium and its effect on fluid flow is modelled on average for this volume. The pressure (inertial effects; form drag) and viscous (skin friction; viscous drag) forces created by the vegetation elements, the so-called drag force, give rise to a momentum sink, causing a deceleration

of the flow (Belcher et al., 2003; Pattanapol et al., 2007). This momentum sink can be modelled with the porous media convention in which the viscous and inertial term are represented by the permeability of the porous medium and by the Forchheimer constant, respectively (Koch et al., 2019; Molina-Aiz et al., 2006; Mahgoub and Ghani, 2021). More commonly is to represent the pressure or form drag as a function of the sectional drag coefficient (C_d) and leaf area density (LAD), because of its meteorological conventions and the specific description of the vegetation's density by LAD (Wilson and Shaw, 1977; Lien et al., 2005). At higher Reynolds number (Re), viscous drag becomes negligible compared with pressure drag (Molina-Aiz et al., 2006) and in many computational fluid dynamics (CFD) models including vegetation, viscous drag is not included (Buccolieri et al., 2018).

Vegetation will generate much higher drag forces than solid elements of similar size and shape, owing to their complex structure and flexible nature. For air flow with Re above approximately 2-7·10^5, plants reach their final form and their C_d becomes independent of Re (Gillies et al., 2002; Molina-Aiz et al., 2006; Poggi et al., 2004). However, very flexible plant species, like desert shrubs (e.g. Greasewood, *Sarcobatus vermiculatis*) or grass-like species (e.g. Fountain Grass, *Pennisetum setaceum*) showed a continuous decrease of C_d with increasing Re (Gillies et al., 2002). Furthermore, C_d values of canopies (both artificial and real) do not become independent of the Reynolds number at high wind speeds, because of the sheltering effect (Lin et al., 2012; Poggi et al., 2004). The latter refers to the shielding of

consecutive leaves which reduces C_d below C_d values of single leaves (Wilson and Shaw, 1977). Therefore, it is important to include vegetation in their real, natural form in wind tunnel setups so that the drag coefficient includes the sheltering effect (Sogachev and Panferov, 2006; Wilson and Shaw, 1977). Different studies demonstrated that C_d varied with plant species, amount of vegetation, its porosity and the flexibility of plant leaves and branches. Thereby, the drag coefficient was experimentally determined by the direct measurement of the drag force on plants (Gillies et al., 2002; Guan et al., 2003) or by velocity-pressure curve data without taking into account the effects of plants on turbulence (Huang et al., 2013; Lin et al., 2012; Molina-Aiz et al., 2006).

Flow separation will occur behind the leaves with formation of vortices in the wake region. It implies the conversion of mean kinetic energy into turbulent kinetic energy (TKE) in the wake region at the larger scales and the breakdown of these large scale eddies to smaller scales (Lien et al., 2005; Sanz, 2003; Wilson and Shaw, 1977). Both 1.5- (E-l closure with E, TKE and l, a predefined mixing length) and two-equation closure models (E-ϕ closure, ϕ mostly representing ϵ, the dissipation of TKE, or ω, the specific dissipation rate (SDR) of TKE) are used to model the mean flow and measures of second-order flow statistics. A great drawback is that the extra terms that are introduced in the turbulence equations are accompanied by additional model constants about which there is great uncertainty. Katul et al. (2004) showed that the E-l equation model of one-dimensional flow

through canopies was more accurate than a k-ϵ turbulence model, due to poor estimation of TKE. Nevertheless, two-equations model are more adequate to model heterogeneous vegetation (Sogachev and Panferov, 2006) and with the right set of model coefficients it reproduces better the velocity and TKE profiles behind the canopy (Zeng et al., 2020). Therefore, many studies tried to find the optimal parameters for k-ϵ (Sanz, 2003; Sogachev and Panferov, 2006; Zeng et al., 2020) and k-ω turbulence models (Sogachev and Panferov, 2006; Sogachev et al., 2012). It was demonstrated that the k-ω model was more accurate in terms of the momentum flux and TKE in the lower canopy than the k-ϵ turbulence model (Pattanapol et al., 2007; Sogachev, 2009). Furthermore, the k-ω model has been demonstrated to have more computational stability and less dependency to lower boundary conditions than the k-ϵ model (Wilcox, 2008). More and more attention goes to the implementation of the source/sink vegetation models into large eddy simulation (LES), which reproduces the flow field around vegetation more accurate than Reynolds-averaged Navier-Stokes (RANS) turbulence models (Lopes et al., 2013). The downsides of LES compared with RANS are the much higher computational cost, the more difficult convergence and the need for calibration of additional input parameters which comes with an extra uncertainty (Kormas et al., 2016; Pan et al., 2014; Salim et al., 2011).

It has been recognised that the accuracy of modelled wind flow is highly linked to uncertainty about the drag coefficient, irrespective of the chosen turbulence model (Pinard and Wilson, 2001). In urban CFD models, drag

coefficients between 0.1 and 0.5 are often used to represent an average drag by a vegetation element (Buccolieri et al., 2018; Tiwary et al., 2006; Bruse and Fleer, 1998), irrespective of the plant species, its LAD or the approaching wind speed. As specified above, there are differences in C_d between plant species (e.g. flexibility) and more important the amount of vegetation and its porosity plays a major role in the aerodynamic effect of plants. This research wants to address the uncertainty of the drag coefficient by looking at the combined effect of vegetation on both the momentum and turbulence equations in CFD models. The drag coefficient will be determined with an optimisation study for a wide range of Reynolds numbers between $3{\cdot}10^3$ and $2.5{\cdot}10^4$, spanning from transitional up to fully turbulent air flow (Çengel et al., 2012). In this way, C_d will include the effect of plants on both the momentum and turbulence balance, something which has not have been reported before to the authors knowledge. The k-ω turbulence model was chosen as a good comprise between model accuracy and computational demand. The plant species under study are climbers commonly found in Western Europe, since they are considered interesting nature-based solutions to mitigate air pollutants and to improve thermal comfort at street scale (Koch et al., 2020; Teotónio et al., 2021; Ysebaert et al., 2021). It is at these so-called street canyons that problems arise owing to reduced natural ventilation with wind speeds lower than 1.5 m s^{-1} (Lauriks et al., 2021). Hence, low wind speed studies are requested and both viscous and form drag effects should be included in the CFD model. Therefore, viscous drag will be regarded during the optimisation

studies. Experimental data will be presented for plant packages, including branches, which were subjected to air flow in a wind tunnel setup. The so-called branch scale incorporates the complex arrangement of leaves and branches in accordance with the plants' real form. At this scale, the aerodynamic properties are approximately uniform so that it can be regarded as a porous medium in CFD models (Huang et al., 2013). This research wants to provide more insight in the accurate aerodynamic characterisation of vegetation in urban CFD models, especially in street canyons characterised by low wind speed conditions. This is critical when modelling the urban heat island effect and pollution dispersion in cities. More so, nature-based solutions to redesign cities for liveability, resilience and sustainability can be examined more precise.

2. Materials and methods

2.1. Wind tunnel experiments

The setup consisted of a closed-circuit wind tunnel with an inner diameter of 103 mm and a total length of 6 m (Figure 1). Plant material was placed in a removable duct with a length of 0.55 m and was kept in place by a screen at both sides. An inline duct fan (Ruck RS-series) with variable controller generated wind speeds from 1.65 ± 0.01 up to 3.81 ± 0.04 m s^{-1} in an empty wind tunnel, i.e. without plants introduced in the designated section. To obtain even lower wind speeds, one or three filter layers (FM10 Calgon Corp

ACF filter) were introduced in the wind tunnel after the plant section (Figure 3, left). The filter layers resulted in an increased pressure drop in the system and thereby a lowering of the wind speed below the minimum wind speed provided by the fan. In this way, wind speeds between 0.40 and 1.03 ± 0.01 m s^{-1} (3 filter layers) and between 1.13 and 1.56 ± 0.02 m s^{-1} (1 filter layer) were reached in the empty wind tunnel, substantially broadening the range of bulk mean wind speed (U_{bulk}) (n=32). For each fan setting, the wind speed in front of the plant section and the pressure drop across the plant section were measured for an empty wind tunnel and for the different species. Wind speed in the empty wind tunnel is regarded as the U_{bulk} of the approaching flow. The associated Re is the bulk Reynolds number and is calculated with the pipe diameter as characteristics length. Temperature and humidity were assumed constant during the experiments, since it was executed in a climate controlled environment, and were, therefore, not considered.

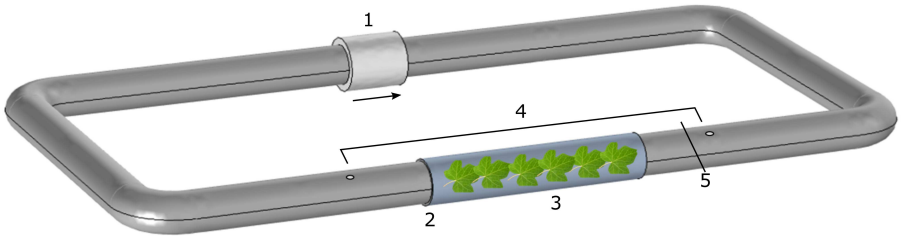

Figure 1: Wind tunnel setup with 1, the inline duct fan, 2, the location of the added filter layers, 3, the removable plant section, 4, the differential pressure sensor, and 5, the air velocity transmitter.

Wind speed was measured in front of the plant section with an air velocity transmitter (CTV 110, Kimo Instruments) with a measuring range from 0 to

30 m s^{-1} and an accuracy of ± 3 %. At that location, air flow measurements were conducted at different heights to obtain the wind speed profile along the cross section. By integrating this profile, the average wind speed, U_{av}, was obtained. The pressure drop across the plant section, including the filter layers, was measured with a differential pressure sensor consisting of a pressure module (700 PD2, Fluke) and a pressure calibrator (717 30G, Fluke) with a resolution of 0.15% over a range of ±7 kPa. The retrieved pressure-velocity curves for the case with filter layers were used to parametrise the model (see section 2.3.2). Figure 2 shows the wind speed measured at different heights for each fan setting in an empty wind tunnel setup. A deviation from fully developed flow can be observed, due to the bend located less then 10 pipe diameters upstream of the wind speed measuring point (Çengel et al., 2012). To take this into account, the complete wind tunnel setup with bends was considered in the geometry of the CFD model.

2.2. Plants

Climbing plants were chosen that are common in temperate regions, namely common ivy (*Hedera helix*), Boston ivy (*Parthenocissus tricuspidata*) and Virginia creeper (*Parthenocissus quinquefolia*) (Figure 4). Realistic plant packages for each species were composed with two different LAD for *H. helix* and *P. tricuspidata*, and one LAD for *Parthenocissus quinquefolia* (Table 3). They were freshly cut and placed in the plant compartment in such a way that they were hanging in the middle of the compartment with the tip of the

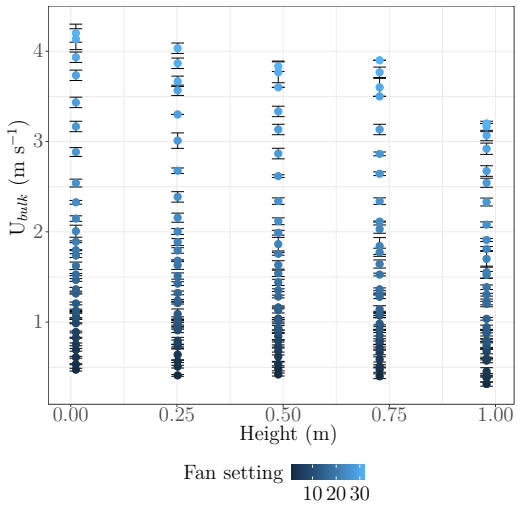

Figure 2: The wind speed (U_{bulk}, m s^{-1}) measured at different heights (H, m) for different fan settings (n=32), which are depicted by the colour legend.

leaves opposing the air flow, as shown on Figure 3 (right).

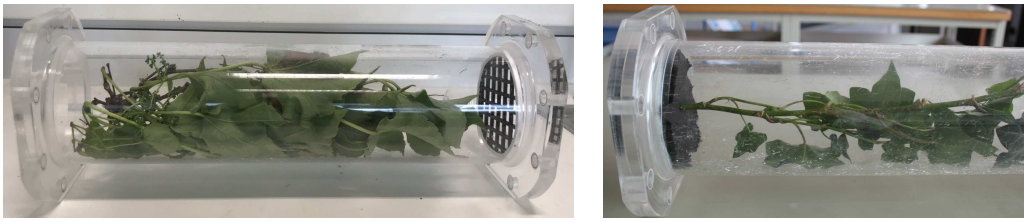

Figure 3: Left: Close-up of of the filter layers that were placed behind the climber packages to decrease overall bulk mean wind speed (U_{bulk}) in the wind tunnel. Right: Example of how the introduction of climber packages (*Parthenocissus tricuspidata*) in the plant section of the wind tunnel was performed. Leaf tips were facing the air flow that passed from right to left.

To understand the behaviour of each species in an air stream, different plant morphological parameters were determined based on previous research (Koch et al., 2019). The parameters and formulae are given in Table 1. Leaf area (LA) and branch area (BA) (cm^2) are the average surface area of a single

Figure 4: From left to right the climbers under study: Ivy (*Hedera helix*), Boston ivy (*Parthenocissus tricuspidata*) and Virginia creeper (*Parthenocissus quinquefolia*).

one-sided leaf and flexible branch, respectively, and were measured using a leaf area meter (Li-3000, LiCor Biosciences). The area was determined for all leaves and branches of each species tested in the wind tunnel setup by 5 replicate measurements. The leaf area measurements were averaged for each species and afterwards used to calculate the leaf dissection index (LDI), functional leaf size (FLS) and LAD. The leaf's complexity can be described by the LDI with a high value for a complex shaped leaf and lower values for a spherical leaf with a minimum of $2\sqrt{\pi}$ (i.e. a sphere). LDI is the ratio of the leaf's perimeter (P_{leaf}) to the root of LA. The FLS gives an idea of the boundary layer development and is defined as the ratio of the largest circle within the boundaries of the leaf (A_{circle}) to LA. The leaf perimeter and circle were determined with ImageJ (version 1.53K), using pictures taken with a Canon Eos 500D camera. Three random leaves for each species were measured 5 times. An important parameter when modelling air flow through plants is the LAD, since it describes vegetation drag better than the frontal area (Molina-Aiz et al., 2006). It is expressed as the total one-sided leaf area per volume occupied by the vegetation (V_{plant}) and has units m^2 m^{-3}

(Buccolieri et al., 2018; Ysebaert et al., 2021). V_{plant} is calculated as the cross-sectional area of the wind tunnel pipe times the thickness of the plant sample in the flow direction. Some authors have reported the use of a plant area density, which includes branch area next to one-sided leaf area, since the combination of branches and leaves will define the influence on air flow (Koch et al., 2020). In this study, the branch area of flexible stems was included in the calculation of the total one-sided leaf area, because of its ability to bend when air flows passes.

Pressure measurements were first normalised with respect to the kinetic energy and LAD before performing statistical analysis. This normalised pressure drop (unitless) was calculated as follows:

$$dP_{norm} = \frac{dP_{stat}}{\frac{1}{2}\rho U_{av}^2 LADL} \tag{1}$$

with dP_{stat} (Pa), the static pressure drop across the plants with length L parallel to the air flow (=0.545 m) and with a certain LAD. $\frac{1}{2}\rho U_{av}$ is the dynamic pressure with ρ, the air density at 20°C (=1.2044 kg m^{-3}) and U_{av} (m s^{-1}), the wind speed of the approaching air flow, averaged across the cross sectional area (Gromke, 2011).

Table 1: Plant morphological parameters determined on the climber species in this study were LA, leaf area, BA, branch area, LDI, leaf dissection index, FLS, functional leaf size and LAD, leaf area density. The formula and unit are given for each parameter with A_{leaf}, single leaf surface area, A_{branch}, single branch surface area, P_{leaf}, leaf perimeter, A_{circle}, largest circle within leaf boundaries, A_{plant}, total one-sided leaf and branch area, and V_{plant}, volume occupied by the plant.

Parameter	Formula	Unit
LA	A_{leaf}	cm^2
BA	A_{branch}	cm^2
LDI	$\frac{P_{leaf}}{\sqrt{A_{leaf}}}$	unitless
FLS	$\frac{A_{circle}}{A_{leaf}}$	unitless
LAD	$\frac{A_{plant}}{V_{plant}}$	$m^2\ m^{-3}$

2.3. Numerical model

2.3.1. Wind tunnel model

Fluid flow was modelled with Comsol Multiphysics (version 5.6) by solving the 3D incompressible, steady Reynolds-averaged Navier-Stokes (SRANS) equation (eqn. 2, conservation form) together with the continuity equation (eqn. 3, conservation form) using a finite element method. A steady state solution was assumed.

$$\rho \boldsymbol{u} \cdot \nabla \boldsymbol{u} = \nabla \cdot (-p\boldsymbol{I} + (\mu + \mu_T)(\nabla \boldsymbol{u} + (\nabla \boldsymbol{u})^T)) + S_{\boldsymbol{u}} \tag{2}$$

$$\rho \nabla \cdot (\boldsymbol{u}) = 0 \tag{3}$$

with $\boldsymbol{u}$ (m s^{-1}), the wind velocity in the x-, y- and z-direction, p (Pa), the pressure, $\boldsymbol{I}$, the identity matrix, μ (kg m^{-1} s^{-1}), the air dynamic viscosity, μ_T, the eddy viscosity (kg m^{-1} s^{-1}) and $S_{\boldsymbol{u}}$, the momentum sink term generated by vegetation. This aspect is considered in section 2.3.3.

The Reynold stress tensor was modelled using the Wilcox revised k-ω turbulence model with k, the TKE, and ω, the SDR (Wilcox, 2008). With the assumption of the Boussinesq approximation, TKE (kg m^{-1} s^{-3}, eqn. 4) and SDR (kg m^{-3} s^{-2}, eqn. 5) are formulated as:

$$\rho \boldsymbol{u} \cdot \nabla k = P_k - \beta^* \rho k \omega + \nabla \cdot ((\mu + \sigma^* \mu_T) \nabla k) + S_k \tag{4}$$

$$\rho \boldsymbol{u} \cdot \nabla \omega = \alpha \frac{\omega}{k} P_k - \beta \rho \omega^2 + \nabla \cdot ((\mu + \sigma \mu_T) \nabla \omega) + S_\omega \tag{5}$$

with P_k, the transfer rate of turbulence kinetic energy from the mean flow to the turbulence (i.e. production of TKE). The closure coefficients and auxiliary relations are defined as (Kormas et al., 2016; Kubacki et al., 2013; Wilcox, 2008): α=$\frac{13}{25}$, β^*=$\frac{9}{100}$, σ=$\frac{1}{2}$, σ^*=$\frac{1}{2}$, β=$\beta_0 \mathrm{f}_\beta$, β_0=$\frac{13}{125}$, $\mathrm{f}_\beta = \frac{1+70\chi_\omega}{1+80\chi_\omega}$, χ_ω=$\frac{\Omega_{ij}\Omega_{jk}S_{ki}}{(\beta_0^*\omega)^3}$ and β^*=$\frac{9}{100}$. The eddy viscosity of the k-ω model is defined as: $\mu_T = \rho \frac{k}{\tilde{\omega}}$ with $\tilde{\omega} = max(\omega, C_{lim}\sqrt{2S_{ij}S_{ij}/\beta^*})$ acting as a stress delimiter (Wilcox, 2008).

2.3.2. Resistance model

The filter layers were inserted to lower the average wind speed in the wind tunnel setup and this is accompanied by an increased pressure drop in the system. This pressure drop can be represented by the Darcy-Forchheimer relation (eqn. 6), which was successfully implemented in a CFD model by Roegiers and Denys (2019) for the same filter layers.

$$\frac{\Delta P}{\Delta x} = -\frac{\mu}{K}U - \beta\rho U^2 \tag{6}$$

with ΔP (Pa), the measured pressure drop across the filter layers, Δx (m), the length of the resistance, here the filter layer thickness, μ (Pa s), the dynamic viscosity, and u, the spatially averaged (Darcian) velocity measured in front of the filter layers which is the product of the filters' porosity (-) and the air velocity. The hydraulic permeability K (m^2) and the Darcy-Forchheimer parameter β (m^{-1}) are determined with the measured pressure-velocity curves. It gives the following set for (K,β): ($8.82 \cdot 10^{-11}$ m^2, 73549 m^{-1}) for one filter layer and ($1.94 \cdot 10^{-10}$ m^2, 77604 m^{-1}) for three filter layers.

2.3.3. Vegetation model

To simulate the influence of vegetation on fluid flow, additional source and sink terms are added to the momentum (eqn. 2), TKE (eqn. 4) and SDR (eqn. 5) equation. The sink term added to the momentum balance $S_{\boldsymbol{u}}$ (eqn.

7) is described by the drag force, which consists of the linear combination of viscous and inertial forces, respectively the first (S_K) and second term (S_{C_d}) in equation 7. The viscous force is described by the permeability of the plant material, permeability (K) (m^2), which indicates how easily air will flow through a vegetation package. The lower K, the more the vegetation package will obstruct the flow and, thus, will generate more viscous drag.

$$\begin{aligned} S_{\boldsymbol{u}} &= -S_K - S_{C_d} \\ &= -\frac{\mu}{K}\boldsymbol{u} - \rho LADC_d U\boldsymbol{u} \end{aligned} \tag{7}$$

with $\boldsymbol{u}$ (m s^{-1}), the wind velocity, μ (Pa s), the dynamic viscosity, K (m^2), the permeability of the plant material, U (m s^{-1}), the spatially averaged wind speed ($U = (u_i u_i)^{0.5}$), LAD (m^2 m^{-3}), the leaf area density, and C_d, the average sectional drag coefficient. The turbulence source and sink terms are given by S_k for TKE and by S_ω for SDR as follows:

$$\begin{aligned} S_k &= S_p - S_d \\ &= \rho LADC_d(\beta_p U^3 - \beta_d U k) \end{aligned} \tag{8}$$

$$\begin{aligned} S_\omega &= (C_{\omega 4} S_p - C_{\omega 5} S_d)\frac{\omega}{k} \\ &= \rho LADC_d(C_{\omega 4}\beta_p \frac{\omega}{k} U^3 - C_{\omega 5}\beta_d U\omega) \end{aligned} \tag{9}$$

β_p, β_d, $C_{\omega 4}$, $C_{\omega 4}$ are model coefficients. Sogachev and Panferov (2006) assumed that the production of TKE by the interaction of plants with the air flow (S_p) is immediately balanced by its dissipation into heat (S_d), meaning that $S_p = S_d$ and S_p can be removed from the balance, so that $C_{\omega 4}$ equals zero. With this assumption, they derived a new formulation for $C_{\omega 5}$ using model constants already present in the k-ω model, namely: $C_{\omega 5} = (C_{\omega 2} - C_{\omega 1})$. This resulted in better representation of the turbulence scale in the lower canopy. Based on this, the following model constants were used: ($\beta_p = 1.0$, $\beta_p = 1.0$, $C_{\omega 4} = 0$, $C_{\omega 5} = (\frac{13}{25} - 0.833)$). The Navier-Stokes equations are solved separately from the turbulence equations using a direct numerical solver with a tolerance of 10^{-6}.

2.3.4. Boundary conditions, Grid convergence and model validation

For each fan setting for which wind speed and pressure drop measurements were performed (both for an empty wind tunnel and a case filled with the different plant species), a fan curve boundary condition was introduced in the wind tunnel model to initiate wind flow. The fan curve consisted of the pressure drop and flow rate of all measurements. Using this fan curve boundary condition, the model will automatically select the working point of the fan as was done by Koch et al. (2019, 2020).

Each grid was constructed of tetrahedral cells with a refined grid at the walls and in the domains of the plants, filter layer and the surface of the

pressure and velocity measurements. Boundary layers were introduced with a thickness adjustment factor of 2.5. A grid convergence study was performed for the empty wind tunnel for a measured wind speed of 0.8 and 2.6 m s^{-1}, corresponding to a case with and without filter layer. Using Richardson interpolation, the (spatial) discretisation error (DE) of the average wind speed at the location of the wind speed measurements in the wind tunnel was retrieved. The grid convergence index (GCI) was calculated with respect to the finest grid with a factor of safety F_s equal to 3 (Franke et al., 2007; Roache, 1994). The results are shown in Table 2.

Table 2: Results of the grid convergence study for the case without and with filter layers in an empty wind tunnel, in terms of the discretisation error (DE) and the grid convergence index (GCI) with respect to the finest grid with F_s=3.

Case	Number of cells	Wind speed (m s^{-1})	DE (%)	GCI (%)
No filter	101,912	2.602	0.5	
No filter	369,520	2.599	0.1	
No filter	606,613	2.598	0.08	0.01
Filter	166,633	0.676	0.9	
Filter	278,357	0.672	0.6	
Filter	634,949	0.669	0.2	0.3

The k-ω model without vegetation, with Darcy-Forchheimer relation for the case with resistance, was first compared against the measured wind speed at the same location in the wind tunnel (represented by number 5 in Figure 1). The model was able to correctly simulate the air flow in the empty wind tunnel setup (Figure 5, left graph). It could also capture the deviation from fully developed flow caused by the pipe bends in the wind tunnel setup

(Figure 5, right graph), however discrepancies between experimental and modelled wind speed were witnessed for the case without filter layer at a normalised height (= $\frac{H}{0.5D}$ with H, the height normal to the flow (m) and D, the pipe diameter (0.0515 m)) of 0 and 0.75 m. For the case with filter layer, less discrepancies were seen. Overall, the model was in fair agreement with the experimental determined wind speed, especially if we look at the average wind speed, and the model can be used to implement the influence of vegetation.

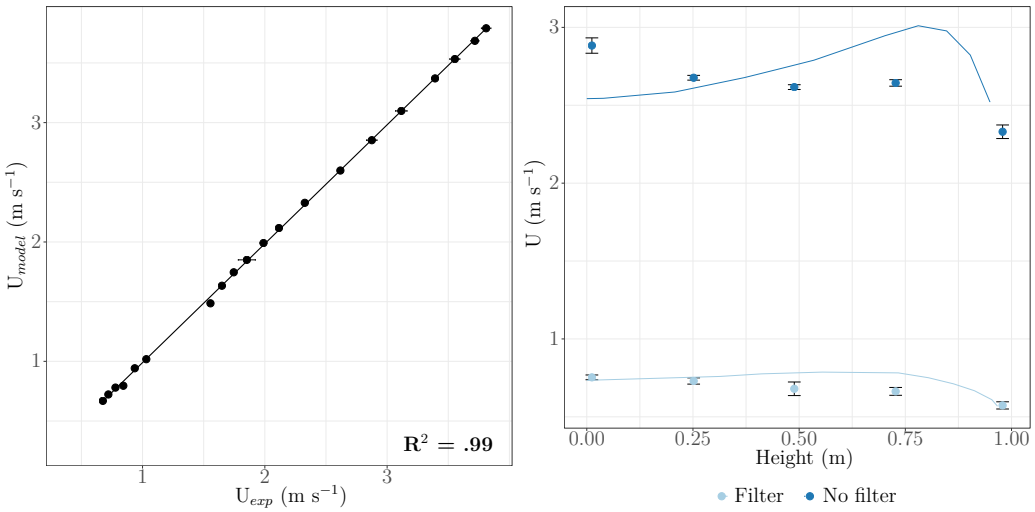

Figure 5: Left graph: Modelled (U_{model}) versus experimentally (U_{exp}) determined wind speeds in an empty wind tunnel. Right graph: The wind speed measured (bullet points) and modelled (full lines) normal to the air flow at different normalised heights for the case with and without filter layers introduced in the wind tunnel setup.

2.3.5. Optimisation

A Nelder-Mead optimisation was utilised with an optimality tolerance of 0.01 to find the value of C_d and K so that the modelled pressure drop matches

the measured pressure drop across the plant section. The objective function therefore takes the following form:

$$\min(dP_{exp} - dP_{model})^2 \tag{10}$$

with dP_{exp} and dP_{model} (Pa), the measured and modelled pressure drop across the plant section, respectively.

The range of values C_d could assume during optimisation was [0;1.5], according to values found in the literature (Gillies et al., 2002; Lin et al., 2012; Molina-Aiz et al., 2006). The lowest value of K was calculated for each species and LAD from pressure-velocity measurements for which a linear relation between pressure drop and wind speed existed meaning that only viscous drag of the plants was acting on air flow. Hence, the quadratic velocity term in equation 7 was eliminated. The maximum value of K was set equal to the dynamic viscosity of air at 20°C ($=1.814 \cdot 10^{-5}$), since at this point viscous drag is equal to the wind speed and is therefore negligible compared to form drag which scales to the square of the wind speed (eqn. 7).

2.4. Statistical analysis

All statistical analysis were conducted with RStudio (version 4.0.3). First, the replicate measurements (n=3) of normalised pressure drop for each species and the blanco were averaged for different U_{bulk} (n=32). Secondly, a natural

log transformation was performed on the normalised pressure drop (dP_{norm}, eqn. 1) to obtain homoscedasticity and linearity of the data. This was checked post-hoc with the regression diagnostics plots and the Shapiro-Wilk normality test. A simple linear regression was constructed to investigate the influence of plant species, wind speed and its interaction on the dP_{norm} and this model was verified with one-way analysis of variance (ANOVA). In addition, the significant morphological parameters, namely LA, BA, LDI and FLS determining the normalised pressure drop were identified with a multiple linear regression (MLR) model, of which its full form with all interactions is given in equation 11. Before performing the MLR, the correlated morphological parameters were determined based on the Spearman's rank correlation coefficients (r_s) and the associated p-value. Subsequently, non-significant interaction terms (p-value < 0.05) were successively removed.

$$y_i = \beta_0 + \beta_1 U_{bulk,i} + \beta_2 LA_i + \beta_3 FLS_i + \beta_4 LDI_i + \beta_5 BA_i + \beta_n interaction_i + \eta_i \tag{11}$$

with y_i, the response variable (here dP_{norm}), β_i, the model coefficients and $\mathrm{U}_{bulk,i}$, LA_i, FLS_i, LDI_i and BA_i, the predictor variables, $\mathrm{interaction}_i$, the interaction terms, and η_i, the error term.

In addition, Spearman's rank correlation coefficients were calculated to identify significant correlations between the morphological characteristics LA, BA, FLS and LDI, and the model parameters K and C_d.

3. Results

3.1. Plant characteristics

P. tricuspidata had the highest leaf area (LA), flexible branch area (BA) and leaf dissection index (LDI) of the three tested species (Table 3). LA and BA was lowest for *P. tricuspidata*. The LDI was comparable for *P. quinquefolia* and *H. helix*, who, therefore, have more spherical leaves compared with *P. tricuspidata*. The largest functional leaf size (FLS) was found for *P. quinquefolia* followed by *P. tricuspidata* and *H. helix*. Spearman's correlation indicated that LA, BA and LDI for the three species were significantly positively correlated (Figure 6). The other plant parameters did not significantly correlate.

Table 3: Measured plant morphological parameters. Leaf area (LA) and branch area (BA) were measured for all leaves that were tested in the wind tunnel and this for two different packing densities, hence different LAD, for *H. helix* and *P. tricuspidata*. Leaf dissection index (LDI) and functional leaf size (FLS) were determined for three random selected leaves.

Parameter	*H. helix*		*P. tricuspidata*		*P. quinquefolia*
LA (cm^2)	27.9 ± 0.1	29.8 ± 0.2	108.8 ± 0.5	98.9 ± 0.5	21.6 ± 0.8
BA (cm^2)	5.08 ± 0.09	5.08 ± 0.09	9.7 ± 0.2	8.8 ± 0.2	2.41 ± 0.02
LDI (-)	4.7 ± 0.1		6.0 ± 0.2		4.6 ± 0.5
FLS (-)	0.44 ± 0.03		0.55 ± 0.04		0.62 ± 0.03
LAD (m^2m^{-3})	6.97 ± 0.01	13.31 ± 0.01	21.30 ± 0.02	48.35 ± 0.02	7.52 ± 0.01

The influence of three climber species on air flow was investigated by examining the pressure drop across the plants for a range of bulk wind speeds (U_{bulk}), which are the mean wind speeds of the approaching flow without

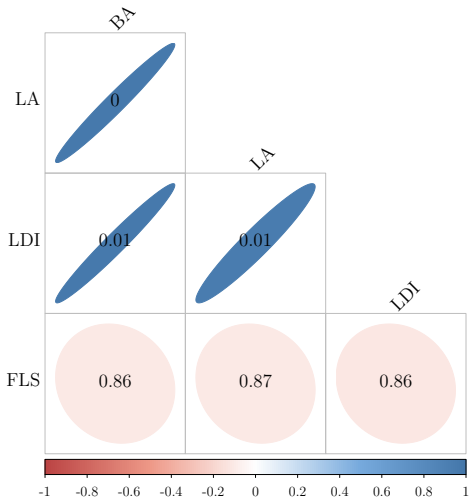

Figure 6: Graphical representation of Spearman's correlation coefficients between the studied morphological parameters LA, leaf area, FLS, functional leaf size, LDI, leaf dissection index, and BA, branch area, ordered following the first principle components. The colour legend shows the Spearman's correlation coefficient r_s and the numbers in the circles the associated p-values.

vegetation (Figure 7). With increasing U_{bulk}, the pressure drop first decreased until a wind speed of 1.56 ± 0.02 (Re =(1.06 ± 0.02)·10^4) for all climbers species. This decrease is attributed to the reduction of the plant's surface area and, thus, viscous drag (so-called static reconfiguration). Subsequently, the pressure drop steadily increased. A quadratic function is plotted through the data for each combination of climber and LAD. The R^2 shows that the quadratic regression does not fit the data well, especially for *P. quinquefolia* and *H. helix* with a LAD of about 7.0 m^2 m^{-3}. The normalised pressure drop dP_{norm} as a function of the Reynolds number for the three climbers decreased with increasing Re, but levelled off for Re$\gtrapprox$4·10^4 at the onset of dynamic reconfiguration by leaf fluttering. At low Reynold numbers and

thus low dynamic pressure (denominator of eqn. 1), little reconfiguration has taken place, resulting in a larger dP_{norm} compared to high Reynolds numbers. In addition, the largest differences in dP_{norm} between climbers was observed at lower Re.

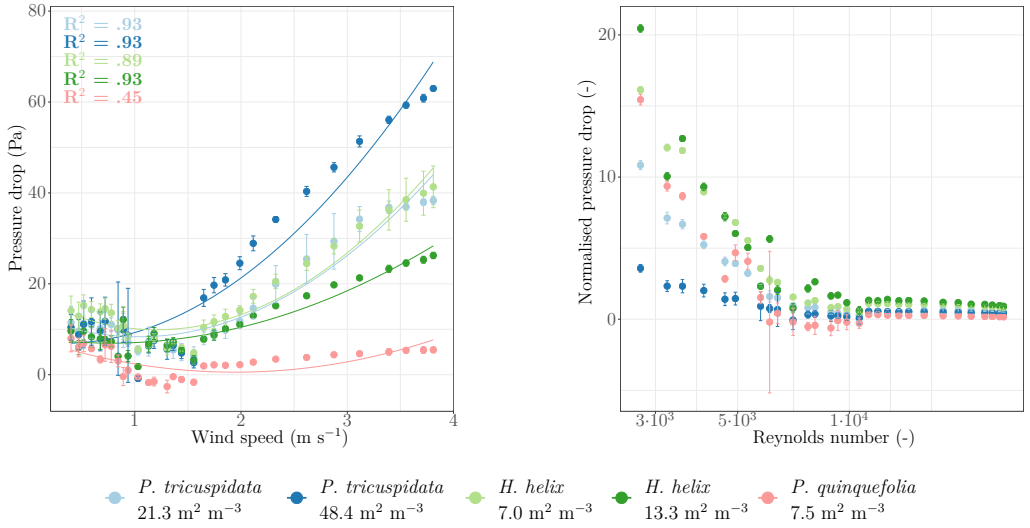

Figure 7: Left graph: Pressure drop (Pa) for each climber as a function of bulk mean wind speed (U_{bulk}), depicted as points. A quadratic fit is shown by the coloured lines and its R^2 for each climber. Right graph: Normalised pressure drop dP_{norm} (unitless) as a function of the Reynolds number, depicted as points. Error bars show the standard deviation of the pressure drop measurements for both graphs.

The effect of the bulk mean wind speed on the normalised pressure drop was not the same for each species, because the interaction term among these two was significant ($p < 0.000001$). Therefore, the data was split for all tested U_{bulk} (n=32) to test the difference in dP_{norm} between the different species. ANOVA showed that dP_{norm} for U_{bulk} between 0.44 ± 0.01 and 1.58 ± 0.01 m s^{-1} was not significantly different between the three species ($p > 0.05$), while this was the case for U_{bulk} between 1.58 ± 0.01 and 3.50 ± 0.04 m s^{-1}

($p < 0.01$). In addition, the data was split for each species to investigate the influence of U_{bulk} on dP_{norm} of each climber. With increasing wind speed, the normalised pressure drop decreased significantly and this decrease was significantly higher for *P. quinquefolia* (p=0.01192) compared with *H. helix* and *P. tricuspidata* (based on the summary output in R, not shown here). The effect of LAD was only significant for *P. tricuspidata* with a lower LAD resulting in lower dP_{norm} values.

Before identifying the morphological parameters that resulted in the distinct difference between species on dP_{norm} (MLR), the correlated parameters were removed. The MLR models for LA, BA and LDI had almost identical R^2 values and it was decided to retain LA, since it is requested to calculate the important model parameter LAD. The stepwise deletion of the non-significant interaction terms resulted in a model without significant interactions (Table 4). It is observed that with increasing U_{bulk}, the normalised pressure drop decreased significantly. Another significant influence is attributed to the functional leaf size, albeit to a lesser extent than U_{bulk}; climbers with a lower FLS give rise to higher normalised pressure drops. On the other hand, LA does not result in significant changes in dP_{norm}.

Table 4: Results of the MLR analysis relating dP_{norm} to the bulk mean wind speed (U_{bulk}), plant species' morphological parameters, leaf area (LA) and functional leaf size (FLS), and interactions among these effects, in terms of the coefficient estimate (after exponential transformation), the standard error (SE) of the coefficient estimate, and the p-value.

Effect	Estimate	SE	p-value
Intercept	76.100	1.43	$1.64 \cdot 10^{-13}$
U_{bulk}	0.501	0.16	$1.71 \cdot 10^{-19}$
LA	0.998	0.037	0.47
FLS	0.004	1.37	$4.06 \cdot 10^{-7}$

3.2. Model results

3.2.1. Permeability and drag coefficient

With increasing Reynolds number, three regions were identified based on the optimisation outcome: (1) a region dominated by viscous drag, (2) a region where both viscous and form drag are at play, (3) a region dominated by form drag. The results will be discussed according to this classification.

Region of viscous drag Permeability was calculated from pressure-velocity measurements with a bulk Reynolds number <4,000. Below this Re, viscous drag was dominating as compared to form drag and K was determined as the coefficient of the linear regression between pressure drop and wind speed following equation 7. This is justified since only the drag coefficient has an impact on the turbulence statistics. The calculated K and R^2 of the linear regression are given in Table 5. Different values for permeability were found for the three climber species with in descending order: *P. quinquefolia* > *H.*

helix > *P. tricuspidata*. Between species, a higher LAD resulted in a lower K value, which implies that air flow is more resisted with higher LAD. For this region, a Spearman's rank correlation analysis was utilised to identify the correlations between the morphological characteristics LA, BA, FLS and LDI and the model parameter K. Significant negative correlations were found between K and LA (r_s = -0.69, p = 0.0004), BA (r_s = -0.65, p = 0.0011), LDI (r_s=-0.64,p = 0.0012) and LAD (r_s =-0.60, p = 0.0029). This is in line with previous results showing the significant correlations between LA, BA and LDI.

Table 5: Calculated permeability (K) for the different plant species and leaf area densities (LAD) with R^2 of the linear regression.

Species	LAD (m^2 m^{-3})	K (m^2)	R^2
Hedera helix	6.97 ± 0.01	$6.39 \cdot 10^{-8}$	0.99
	13.31 ± 0.01	$5.74 \cdot 10^{-8}$	0.99
Parthenocissus tricuspidata	21.30 ± 0.02	$5.95 \cdot 10^{-8}$	0.99
	48.35 ± 0.02	$5.32 \cdot 10^{-8}$	0.99
Parthenocissus quinquefolia	7.52 ± 0.01	$6.50 \cdot 10^{-8}$	0.99

Region of viscous and form drag For Re > 4,000 and < 10,000, the optimisation study searched for the one combination of permeability and drag coefficient that resulted in the experimentally determined pressure drop for each climber. Optimisations with an objective function of 7.5 were retained as valid result, since optimising for two variables was more complex. It corresponds to a deviation of 25% between modelled and measured results, i.e. a fair agreement (Blocken et al., 2012). The experimental pressure drop of

certain climbers and wind speeds was negative, hence for these cases an optimisation study could not be performed. In the end, optimisation results were obtained for *H. helix* 7.0 m^2 m^{-3} (n=5), *H. helix* 13.3 m^2 m^{-3} (n=5), *P. tricuspidata* 21.3 m^2 m^{-3} (n=8), *P. tricuspidata* 48.4 m^2 m^{-3} (n=5), *P. quinquefolia* 7.5 m^2 m^{-3} (n=5). Figure 8 shows K and C_d obtained by the optimisation study for different Reynolds numbers. For each climber, K increased with increasing Re and it approaches the dynamic viscosity of air at Re values specific for each climber and LAD. This shift from viscous to form drag is further illustrated by Figure 9, showing the proportion of the momentum sink $S_{\boldsymbol{u}}$ related to viscous drag (S_K) and form drag (S_{C_d}), as depicted in equation 7. The inflection point between viscous and form drag is at Re$\cong 6.2 \cdot 10^3$ for *H. helix* with LAD of 7.0 m^2 m^{-3} and *P. quinquefolia* with LAD of 7.5 m^2 m^{-3} in comparison with the other three cases, where inflection takes place at Re$\cong 9.6 \cdot 10^3$. Therefore, it is suggested that LAD is determinant for the inflection point between viscous and form drag irrespective of the type of climber. For all cases, permeability follows a logistic function of the form $A_{sym}/(1+exp(x_{mid}-Re/scale))$, with A_{sym}, x_{mid}, $scale$ representing the asymptote, the Re value at the inflection point of the curve, and a numeric scale parameter, respectively (SSlogis function in RStudio). The equations are given in Table 6 and plotted on Figure 8 (dashed lines). The evolution of C_d with increasing Re in this region is not unambiguous and its value fluctuates a lot. In this region, viscous an form drag forces alternate, depending on flow disturbances, hence it is not possible to obtain

reliable C_d values in this transition region.

Table 6: Logistic function equation between permeability (K) and Reynolds number (Re) for the different climber species and leaf area densities (LAD).

Species	LAD (m^2 m^{-3})	K equation (m^2)
H. helix	6.97 ± 0.01	$1.814 \cdot 10^{-5}/(1+\exp((6.52 - Re)/0.31 \cdot 10^3))$
	13.31 ± 0.01	$1.814 \cdot 10^{-5}/(1+\exp((9.41 - Re)/0.09 \cdot 10^3))$
P. tricuspidata	21.30 ± 0.02	$1.814 \cdot 10^{-5}/(1+\exp((9.86 - Re)/0.1 \cdot 10^3))$
	48.35 ± 0.02	$1.814 \cdot 10^{-5}/(1+\exp((9.56 - Re)/0.12 \cdot 10^3))$
P. quinquefolia	7.52 ± 0.01	$1.814 \cdot 10^{-5}/(1+\exp((5.97 - Re)/0.07 \cdot 10^3))$

Region of form drag For Re >10,000, the optimisation study was only performed for C_d (n=14 for each climber) and the objective function was analysed more strictly with a value of 0.01. C_d decreased with increasing Re for all species, but C_d does not reach a constant value at the highest Re. The decline of C_d and Re in this region followed a power law function and its values are shown in Table 7. The graphs are grouped for *Hedera helix* and *P. tricuspidata* with generally higher C_d values for the lowest LAD. Overall, it can be seen that *H. helix* withstands flow the most, followed by *P. tricupidata* and *P. quinquefolia*. It suggested that *P. quinquefolia* reconfigures to a larger extent at high wind speeds compared with the other two climbers. A Spearman's rank correlation analysis was utilised to identify the relations between the morphological characteristics LA, FLS, LDI and BA and the model parameter C_d for this region. Significant negative correlations were found between C_d and LAD (r_s = -0.32, p = 0.0091) and between C_d and FLS (r_s = -0.91, p < 0.0000).

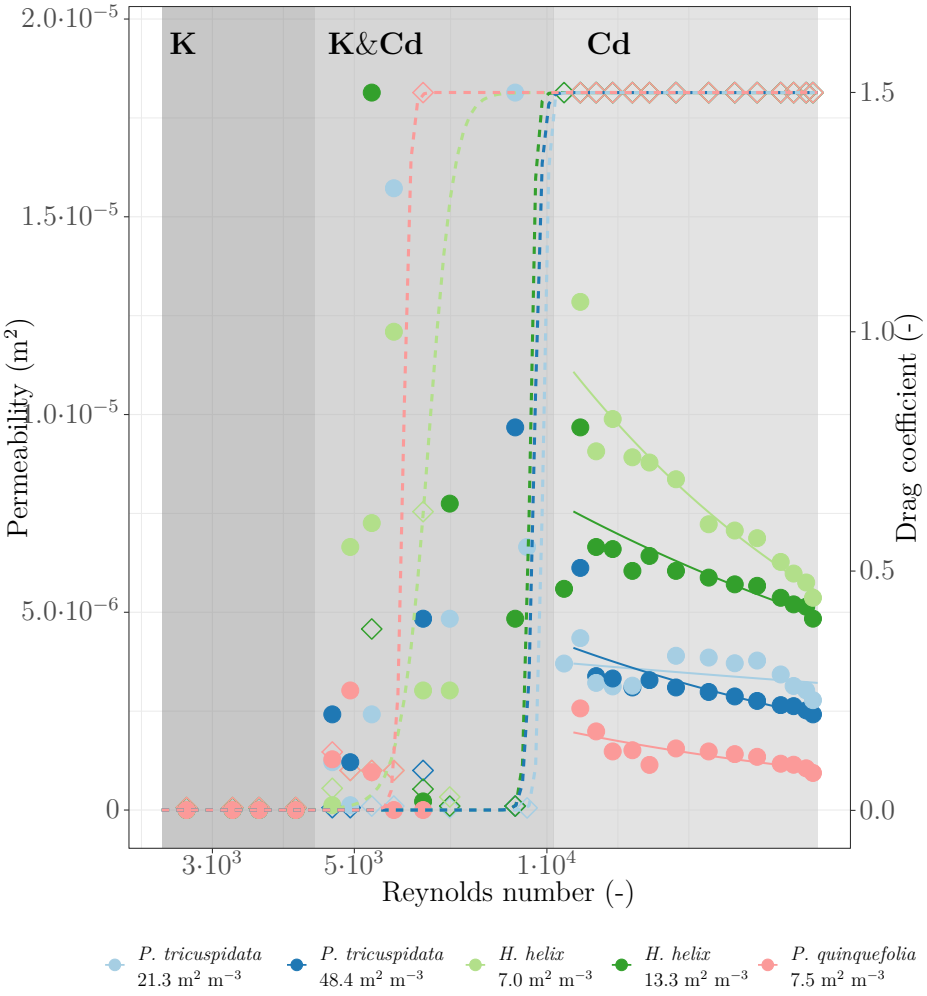

Figure 8: Permeability (m^2) (left axis, represented by open diamond symbols) and drag coefficient (-) (right axis represented by bullet symbols) obtained with model optimisation as a function of the Reynolds number. The region with K (dark grey), K & C_d (lighter grey) and C_d (light grey) refer to the three different regions that were identified in this study for which an optimisation study was performed for K, K and C_d, and C_d, respectively. The colour legend refers to the combination of climber species and LAD, as given in Table 3. A logistic function is fitted through all K values for each case, represented by the dashed lines, while a power law function is fitted through the C_d data only of the third region, represented by the full lines.

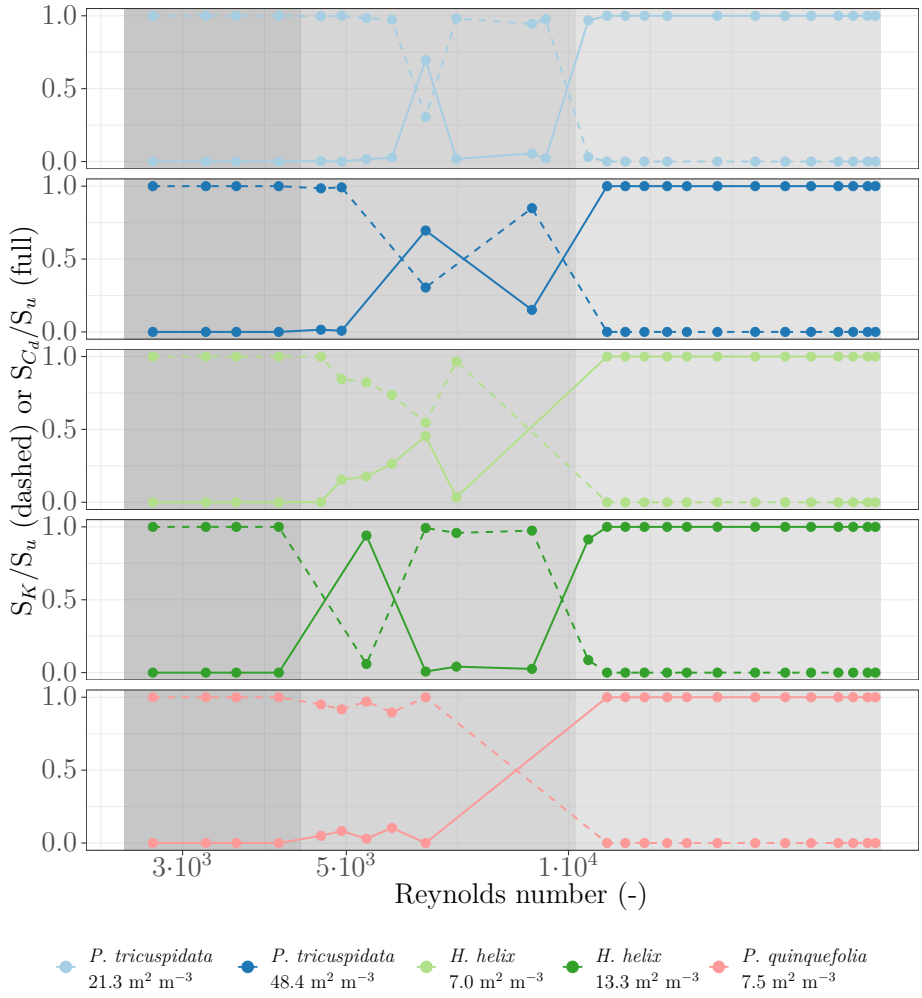

Figure 9: Relative contribution of viscous (S_K) (dashed lines) and form (S_{C_d}) drag (full lines) to the momentum sink ($S_{\boldsymbol{u}}$) caused by climbers. The colour legend refers to the combination of climber species and LAD, as given in Table 3. The dark, lighter and light grey region depict the regions for which an optimisation study was performed for K, K and C_d, and C_d, respectively.

3.2.2. Validation

The optimisation was performed by the comparison of the modelled and measured pressure drop across the plant section. The wind speeds obtained

Table 7: Power law equation between drag coefficient (C_d) and Reynolds number (Re) for the different plant species and leaf area densities (LAD).

Species	LAD (m^2 m^{-3})	C_d equation (-)
Hedera helix	6.97 ± 0.01	$1480 \cdot Re^{-0.79}$
	13.31 ± 0.01	$60.1 \cdot Re^{-0.49}$
Parthenocissus tricuspidata	21.30 ± 0.02	$1.37 \cdot Re^{-0.16}$
	48.35 ± 0.02	$106 \cdot Re^{-0.62}$
Parthenocissus quinquefolia	7.52 ± 0.01	$146 \cdot Re^{-0.79}$

after optimisation of K and C_d approximated the measured wind speeds with a R^2 of above 0.95 for all climber species (Figure 10). The highest deviation was found for wind speeds below 2 m s^{-1} which corresponds to the transition region from viscous to form drag. If C_d was set equal to 0.2, which is common practice to model vegetation in urban CFD models (Buccolieri et al., 2018), the R^2 between modelled and experimental data was on average 0.04 units lower as compared to the wind speed with optimised C_d for all climbers. In addition, the pressure drops differed a lot ($R^2 < 0.2$) Hence, including viscous drag at low wind speeds and using a declining C_d with Re provides a more accurate description of the aerodynamic effect of climbers.

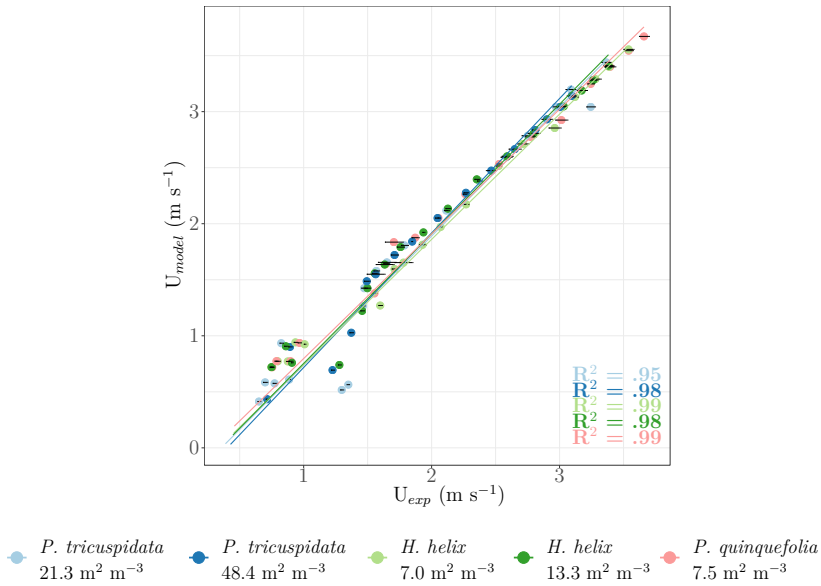

Figure 10: Modelled wind speeds versus experimentally determined wind speeds when climbers are placed in the wind tunnel. Species and LAD are shown by the colour legend (Table 3). For both graphs, dots represent the specific measurement point and the line gives the linear regression, of which the R^2 is also displayed.

4. Discussion

4.1. Plant characteristics

Pressure-velocity results of three climber species, *Hedera helix*, *Parthenocissus tricuspidata* and *Parthenocissus quinquefolia*, were obtained with wind tunnel experiments for a wide range of bulk mean wind speeds from 0.04 ± 0.01 to 3.81 ± 0.04 m s^{-1}. By normalising for the prevalent dynamic pressure, LAD and plant material thickness, differences in pressure drop between climbers could be examined in terms of a normalised pressure drop. The results suggested that functional leaf size (FLS) was a significant plant char-

acteristic influencing air flow. A smaller FLS, equivalent with more elongated leaves, leads to higher normalised pressure drops. It confirms that FLS is a measure for the development of a leaf boundary layer with a decrease in boundary layer thickness for leaves with lower FLS. Previous wind tunnel studies with a range of green wall species (not limited to climbers) (Koch et al., 2019) and with tree and shrub species (Koch et al., 2020) did not reveal any morphological parameters significantly affecting normalised pressure drop. In these studies, plants were subjected to wind speeds from 1.14 to 4.40 m s^{-1}, while this study showed the highest difference between climbers species at wind speeds below 1.5 m s^{-1}. This could explain why a significant influence of FLS was found in this study, nevertheless more species, including other type of green wall, shrub and tree species, should be tested at lower wind speeds to corroborate these findings. On the other hand, the finding that elongated leaves impede air movement to a greater extent was consisting with pollutant reduction studies that show more capture of particulate matter by smaller-leaved and needle-leaved species as a result of the reduced leaf boundary layer thickness (Freer-Smith et al., 2005; Muhammad et al., 2019; Weerakkody et al., 2018). Notwithstanding, leaves with narrow leaf bases bend easily with wind flow and demonstrated less particle deposition (Leonard et al., 2016). However, this is not quantified with FLS. Leaf area (LA), branch area (BA), and leaf dissection index (LDI) were correlated to each other, but did not significantly affect normalised pressure drop. This was corroborated by PM deposition studies that showed no relation between

net particle accumulation and a leaf's area and complexity (represented by LDI) (Muhammad et al., 2019; Leonard et al., 2016; Weerakkody et al., 2018).

In our study, a higher LAD for *P. tricuspidata* resulted in lower pressure drops that were significantly different, which is caused by sheltering of front leaves and is in line with Molina-Aiz et al. (2006). Using pressure-velocity curves, the latter authors obtained C_d values between 0.15 and 0.35 for 5 different greenhouse crops. In addition, raising the wind speed significantly lowered the normalised pressure drop for all species and this is attributed to leaf reconfiguration, i.e. reduction of surface area and streamlining with the wind, which is a common relation found for drag (Gillies et al., 2002; Huang et al., 2013; Lin et al., 2012; Thom, 1969; Wilson and Shaw, 1977).

4.2. Permeability and drag coefficient

The results from the optimisation study clearly showed the influence of both viscous and form drag on the aerodynamic effect of climbers. In general, three regions could be identified in order of increasing bulk Reynolds number: (1) region dominated by viscous drag where the permeability was determined, (2) a region with viscous and form drag effects where both permeability and drag coefficient were determined, and (3) a region dominated by form drag where drag coefficient was determined.

For the first region (Re $<$ 4,000 and U $<$ 0.6 m s^{-1}), the permeability was derived from pressure-velocity measurements and K was smallest for *P. tricuspidata*, followed by *H. helix* and *P. quinquefolia* (averaged for the

two LADs). It suggested that a larger leaved climber produced a higher viscous drag, which was confirmed by the negative correlation between K and LA. Wind tunnel experiments concerning green wall and tree species showed that permeability is significantly correlated with specific leaf area (i.e. LA divided by its dry mass) for green wall species and specific leaf area and LDI for tree species (Koch et al., 2019, 2020). Next to LDI, this study also found a correlation between K and LA, BA and LAD. Between Re of 4,000-10,000 (U = 0.68 - 1.56 m s^{-1}), a transition region was identified in which viscous drag was overtaken by form drag. With increasing wind speed, the permeability declined from around $5{\cdot}10^{-8}$ up to the dynamic viscosity of air ($\approx 10^{-5}$) following a logistic function. The inflection point took place between Re equal to 0.6-1$\cdot 10^4$ depending on the type of climber and its LAD. This corresponds to a wind speed of around 0.8 to 1.5 m s^{-1}. C_d did not show a distinct pattern, which is also observed for the friction factor when going from laminar to turbulent flow in a piping system (Çengel et al., 2012). Beyond the transition region, drag forces are dominated by form drag and the drag coefficient was optimised for. C_d decreased with increasing Re in this region following a power law function. The decline is attributed to the sheltering effect of consecutive vegetation elements (Lin et al., 2012; Poggi et al., 2004). C_d would probably attain a constant value if Re was increased up to levels above $2.5{\cdot}10^4$, as was described in the literature Gillies et al. (2002); Guan et al. (2003); Molina-Aiz et al. (2006).

Overall, the range of drag coefficients obtained with our optimisation

study was 0.01-1.06 for *H. helix* 7.0 m^2 m^{-3}, 0.01-0.8 for *H. helix* 13.3 m^2 m^{-3}, 0.01-1.5 for *P. tricuspidata* 21.3 m^2 m^{-3}, 0.01-0.8 for *P. tricuspidata* 48.3 m^2 m^{-3}, 0-0.25 for *P. quinquefolia* 7.5 m^2 m^{-3}. This varying nature of the drag coefficient demonstrates the necessity to include drag coefficients dependent on wind speeds in CFD models. This study also indicated that the use of C_d=0.2, which is common practice to model the aerodynamic effect of vegetation (Buccolieri et al., 2018), leads to deviations. The optimised C_d values are in agreement with several C_d values reported in the literature. C_d was calculated from force measurements with the relation $C_d = \frac{F}{0.5\rho U^2 A}$ for artificial wind breaks (C_d = 0.6-1.2 for Re=1-4·10^4) and for ornamental grass (C_d = 0.2-0.47), a small leafy shrub (C_d = 0.25-0.48) and a coniferous tree (C_d = 0.28-0.55) for Re= 0.4-5.3·10^4 (Gillies et al., 2002; Guan et al., 2003). Both studies investigated different aerodynamic porosities, which is an estimate of how easily wind can pass vegetation and is, therefore, the opposite of LAD. They found a decrease in C_d with increasing aerodynamic porosity. Likewise, this study demonstrated that both LAD and FLS are negatively correlated with the drag coefficient. Koch et al. (2019) corroborated the significant correlation between Forchheimer constant of green wall species and FLS, with drag coefficients of 0.08-0.52 (converted from Forchheimer constants, which represents form drag like C_d). On the other hand, the Forchheimer constant was not correlated with any morphological parameter for tree species (C_d = 0.03-0.50) (Koch et al., 2020).

Limited studies looked at the interplay of viscous and form drag forces.

Thom (1969) postulated that viscous drag for a single, rigid leaf is only substantial relative to form drag for a leaf parallel with air flow. For other leaf angles, form drag is the main form of drag and it is independent of wind speed above 0.6 m s^{-1}. Molina-Aiz et al. (2006), who studied greenhouse crops in a wind tunnel setup comparable to the one in this research, found that the shift from viscous to form drag occurred for velocities above 2 m s^{-1} ($Re \approx 5 \cdot 10^4$), which is slightly higher than the wind speed found in this study. The main difference is that the permeability and drag coefficient in this study were found with an optimisation to match pressure-velocity curves not only by including a vegetation momentum sink, but also a turbulence sink term. During vegetation-wind interaction, vortices are created in their wake region, so that momentum is converted into specific dissipation rate (SDR) and this explains the lower wind speed at which the shift from viscous to form drag occurs. To conclude, the inclusion of both viscous and form drag forces when modelling the aerodynamic effect of vegetation is necessary, since stagnation zones of wind speeds are commonly found behind buildings and in street canyons. For example, measurements in a Belgian street canyon demonstrated wind speeds below 1.5 m s^{-1} (Lauriks et al., 2021). Furthermore, dissipation of momentum should be included to resolve the influence of vegetation correctly (Zeng et al., 2020).

4.3. Model validation

In a first step, the Wilcox revised k-ω model, including a Darcy-Forchheimer submodel to represent the added filter layers, was validated. The model predicted the mean wind speed in the empty wind tunnel correctly with an R^2 of 0.99. Moreover, the grid convergence index for both the case without and with filter layers was below 1%. Secondly, the optimisation study was able to find an optimal combination for the permeability and drag coefficient for on average 18 different wind speeds for all tested climbers for the three regions. The modelled wind speed agreed with the measured wind speed ($R^2 > 0.95$). The obtained K and C_d values were in agreement with values found in the literature and, therefore, the authors of this research are suggesting that the model coefficients after Sogachev (2009) are able to represent the turbulence sink terms by climbers in a correct manner. In addition, the accuracy of the Sogachev model was already proven for canopy flow from wind tunnel and real tree stands measurements (Sogachev, 2009; Sogachev et al., 2012) and other studies came to the similar conclusions about the turbulence coefficients, i.e. the turbulence sink term should be negative. This is because the turbulence generated by the shear of vegetation elements occurs at scales smaller than the smallest grid cell, so that this turbulence is dissipated before being advected to another cell (Lopes et al., 2013; Zeng et al., 2020). Contradicting these models, the Sogachev model does not include any sink term in the turbulent kinetic energy equation. Nevertheless, accurate description of the drag coefficient is even more crucial to model vegetation-

wind interactions accurately. The correct description of the flow field is key in modelling the PM deposition onto vegetation and the hygrothermal effect of vegetation, among others. In addition, the drag coefficient is used in PM deposition models to calculate the particle turbulent diffusivity (Huang et al., 2013; Lin et al., 2012).

5. Conclusion

This study presented wind tunnel experiments with climbers subjected to a range of Reynolds numbers ($3{\cdot}10^3$ up to $2.5{\cdot}10^4$). The measured pressure-velocity data were used (1) to relate plant morphological parameters to flow resistance and (2) to optimise the permeability and drag coefficient as a function of Re. Firstly, the normalised pressure drop was significantly determined by the functional leaf size, while it was not depending on the leaf area, branch area and leaf dissection index. Secondly, the interplay between K and C_d was unravelled; with increasing bulk mean wind speed, viscous drag was overtaken by form drag at a Reynolds number of approximately $0.6\text{-}1{\cdot}10^4$ and this was accompanied by a decrease of K from $\approx 5{\cdot}10^{-8}$ up to $\approx 10^{-5}$ m^2, while C_d did not show a distinct evolution. Above the transition from viscous to form drag, C_d reached a maximum value after which it steadily declined following a power law function, a result of the sheltering effect. Drag coefficients in the range of 0 up to 1.5 were obtained. The present study clearly demonstrated that the model with optimised parameters was

superior to conventional CFD models using $C_d = 0.2$. Hence, it is critical that urban CFD models include both viscous and form drag effects of vegetation in terms of a varying K and C_d with wind speed by a logistic and power function, respectively. It would also improve the modelling of the urban heat island effect and pollution dispersion in cities, so that nature-based solutions can be deployed to a greater extent. Moreover, the plant morphological parameters that significantly correlate with drag were ascertained. Both LAD and FLS were negatively correlated with C_d, while a negative correlation existed between LA, BA, LDI and LAD and K.

However, the amount of species and their LAD was limited, so the found correlations between plant morphological parameters and resistance to air flow should be verified with further studies. Especially, the influence of LAD was found to be influential on both permeability and drag coefficient by the present study and this relation should be studied in more detail. In addition, the present study only used the mean wind speed in front of the vegetation to find the optimal parameters determining vegetation's viscous and form drag, however these coefficients are also determining the turbulence statistics. Future work should include turbulence kinetic energy measurements behind the plants to verify if the parametrisation is also resulting in correct simulation of turbulent kinetic energy and specific dissipation rate. Furthermore, turbulence will also have an influence on the drag coefficients and it would be interesting to investigate the relationship between them. Although, the influence of turbulence will probably be included in the dependency of the drag

coefficients with the wind speed, since turbulent kinetic energy (TKE), specific dissipation rate (SDR) and the Reynolds number (Re) are all correlated.

Acknowledgements

T.Y. is supported as doctoral candidate (Strategic basic research) from the Research Foundation - Flanders (FWO, 1S88919N).

References

Belcher, S. E., Jerram, N., Hunt, J. C. R., 2003. Adjustment of a turbulent boundary layer to a canopy of roughness elements. Journal of Fluid Mechanics 488, 369–398.

Blocken, B., Janssen, W., van Hooff, T., 2012. CFD simulation for pedestrian wind comfort and wind safety in urban areas: General decision framework and case study for the eindhoven university campus. Environmental Modelling & Software 30, 15–34.

Bruse, M., Fleer, H., 1998. Simulating surface-plant-air interactions inside urban environments with a three dimensional numerical model. Environmental Modelling & Software 13, 373–384.

Buccolieri, R., Santiago, J.-L., Rivas, E., Sanchez, B., 2018. Review on urban tree modelling in cfd simulations: Aerodynamic, deposition and thermal effects. Urban Forestry & Urban Greening 31, 212–220.

Çengel, Y. A., Cimbala, J. M., Turner, R. H., 2012. Fundamentals of Thermal Fluid Sciences, fifth edition Edition. McGraw-Hill Education.

Franke, J., Hellsten, A., Schlünzen, H., Carissimo, B., 2007. Best practice guideline for the cfd simulation of flows in the urban environment. Brussels: COST Office.

Freer-Smith, P. H., Beckett, K. P., Taylor, G., 2005. Deposition velocities to sorbus aria, acer campestre, populus deltoides × trichocarpa 'beaupré', pinus nigra and × cupressocyparis leylandii for coarse, fine and ultra-fine particles in the urban environment. Environmental Pollution 133 (1), 157–167.

Gillies, J. A., Nickling, W. G., King, J., 2002. Drag coefficient and plant form response to wind speed in three plant species: Burning bush (*Euonymus alatus*), colorado blue spruce (*Picea pungens glauca.*), and fountain grass (*Pennisetum setaceum*). Journal of Geophysical Research Atmospheres 107, 1–15.

Gromke, C., 2011. A vegetation modeling concept for building and environmental aerodynamics wind tunnel tests and its application in pollutant dispersion studies. Environmental Pollution 159 (8-9), 2094–2099.

Guan, D., Zhang, Y., Zhu, T., 2003. A wind-tunnel study of windbreak drag. Agricultural and Forest Meteorology 118, 75–84.

Huang, C.-W., Lin, M.-Y., Khlystov, A., Katul, G., 2013. The effects of leaf area density variation on the particle collection efficiency in the size range

of ultrafine particles (UFP). Environmental Science & Technology 47 (20), 11607–11615.

Katul, G. G., Mahrt, L., Poggi, D., Sanz, C., 2004. One- and two-equation models for canopy turbulence. Boundary-Layer Meteorology 113, 81–109.

Koch, K., Samson, R., Denys, S., 2019. Aerodynamic characterisation of green wall vegetation based on plant morphology: An experimental and computational fluid dynamics approach. Biosystems Engineering 178, 34–51.

Koch, K., Ysebaert, T., Denys, S., Samson, R., 2020. Urban heat stress mitigation potential of green walls: A review. Urban Forestry & Urban Greening 55, 126843.

Kormas, A., Prospathopoulos, J. M., Chaviaropoulos, P. K., Yakinthos, K., 2016. Wind flow simulation over forested areas using a 3d RANS solver with a tree – scale approach. Journal of Wind Engineering and Industrial Aerodynamics 155, 149–158.

Kubacki, S., Rokicki, J., Dick, E., 2013. Hybrid RANS/LES computations of plane impinging jets with DES and PANS models. International Journal of Heat and Fluid Flow 44, 596–609.

Lauriks, T., Longo, R., Baetens, D., Derudi, M., Parente, A., Bellemans, A., van Beeck, J., Denys, S., 2021. Application of improved CFD modeling

for prediction and mitigation of traffic-related air pollution hotspots in a realistic urban street. Atmospheric Environment 246, 118127.

Leonard, R. J., McArthur, C., Hochuli, D. F., 2016. Particulate matter deposition on roadside plants and the importance of leaf trait combinations. Urban Forestry & Urban Greening 20, 249–253.

Lien, F.-S., Yee, E., Wilson, J. D., 2005. Numerical modelling of the turbulent flow developing within and over a 3-d building array, part ii: a mathematical foundation for a distributed drag force approach. Boundary-Layer Meteorology 114, 245–285.

Lin, M., Katul, G. G., Khlystov, A., 2012. A branch scale analytical model for predicting the vegetation collection efficiency of ultrafine particles. Atmospheric Environment 51, 293–302.

Lopes, A. S., Palma, J. M. L. M., Lopes, J. V., 2013. Improving a two-equation turbulence model for canopy flows using large-eddy simulation. Boundary-Layer Meteorology 149 (2), 231–257.

Mahgoub, A. O., Ghani, S., 2021. Numerical and experimental investigation of utilizing the porous mediamodel for windbreaks cfd simulation. Sustainable CIties and Society 65, 102648.

Molina-Aiz, F. D., Valera, D. L., Álvarez, A. J., Madueño, A., 2006. A wind tunnel study of airflow through horticultural crops: Determination of the drag coefficient. Biosystems Engineering 93, 447–457.

Muhammad, S., Wuyts, K., Samson, R., 2019. Atmospheric net particle accumulation on 96 plant species with contrasting morphological and anatomical leaf characteristics in a common garden experiment. Atmospheric Environment 202, 328–344.

Pan, Y., Chamecki, M., Scott, A., 2014. Large-eddy simulation of turbulence and particle dispersion inside the canopy roughness sublayer. Journal of Fluid Mechanics 753, 499–534.

Pattanapol, W., Wakes, S. J., Hilton, M. J., Dickinson, K. J. M., 2007. Modeling of surface roughness for flow over a complex vegetated surface. International Journal of Environmental and Ecological Engineering 1 (8), 94–102.

Pinard, J. D. J.-P., Wilson, J. D., 2001. First- and second-order closure models for wind in a plant canopy. Journal of Applied Meteorology 40, 1762–1768.

Poggi, D., Porporato, A., RIidolfi, L., 2004. The effect of vegetation density on canopy sub-layer turbulence. Boundary-layer Meteorology 111, 565–587.

Roache, P. J., 1994. Perspective: a method for uniform reporting of grid refinement studies. Journal of Fluids Engineering 116, 405–413.

Roegiers, J., Denys, S., 2019. CFD-modelling of activated carbon fibers for indoor air purification. Chemical Engineering Journal 365, 80–87.

Salim, S. M., Cheah, S. C., Chan, A., 2011. Numerical simulation of dispersion in urban street canyons with avenue-like tree plantings: Comparison between RANS and LES. Building and Environment 46 (9), 1735–1746.

Sanz, C., 2003. A note on k - ε modelling of vegetation canopy air-flows. Boundary-Layer Meteorology 108, 191–197.

Sogachev, A., 2009. A note on two-equation closure modelling of canopy flow. Boundary-Layer Meteorology 130 (3), 423–435.

Sogachev, A., Kelly, M., Leclerc, M. Y., 2012. Consistent two-equation closure modelling for atmospheric research: buoyancy and vegetation implementations. Boundary-Layer Meteorology 145 (2), 307–327.

Sogachev, A., Panferov, O., 2006. Modification of two-equation models to account for plant drag. Boundary-Layer Meteorology 121 (2), 229–266.

Teotónio, I., Silva, C. M., Cruz, C. O., 2021. Economics of green roofs and green walls: A literature review. Sustainable Cities and Society 69, 102781.

Thom, A. S., 1969. The exchange of momentum and mass and heat between an and artificial leaf and the airflow in a wind-tunnel. Quarterly Journal of the Royal Meteorological Society 94, 44–55.

Tiwary, A., Hervé, P. M., Colls, J. J., 2006. Modelling the size-dependent collection efficiency of hedgerows for ambient aerosols. Journal of Aerosol Science 37, 990–1015.

Tzoulas, K., Korpela, K., Venn, S., Yli-Pelkonen, V., Kaźmierczak, A., Niemela, J., James, P., 2007. Promoting ecosystem and human health in urban areasusing green infrastructure: A literature review. Landscape and Urban Planning 81, 167–178.

Weerakkody, U., Dover, J. W., Mitchell, P., Reiling, K., 2018. Quantification of the traffic-generated particulate matter capture by plant species in a living wall and evaluation of the important leaf characteristics. Science of The Total Environment 635, 1012–1024.

Wilcox, D. C., 2008. Formulation of the k - ω turbulence model revisited. AIAA Journal 46 (11).

Wilson, N. R., Shaw, R. H., 1977. A higher and order closure and model for canopy and flow. Journal of Applied Meteorology 16 (11), 1197–1205.

Wong, N. H., Tan, A. Y. K., Tan, P. Y., Chiang, K., Wong, N. C., 2010. Acoustics evaluation of vertical greenery systems for building walls. Building and Environment 45 (2), 411–420.

Yang, Y., Xie, Z., Tse, T. K. T., Jin, X., Gu, M., 2012. Verification of a tree canopy model and an example of its application in wind environment optimization. Wind and Structures, An International Journal 15, 409–421.

Ysebaert, T., Koch, K., Samson, R., Denys, S., 2021. Green walls for mitigating urban particulate matter pollution - a review. Urban Forestry & Urban Greening 59, 127014.

Zeng, F., Lei, C., Liu, J., Niu, J., Gao, N., 2020. CFD simulation of the drag effect of urban trees: Source term modification method revisited at the tree scale. Sustainable Cities and Society 56, 102079.